JCTC Journal of Chemical Theory and Computation

Article

pubs.acs.org/JCTC

Computational Investigation on the Spectroscopic Properties of Thiophene Based Europium β-Diketonate Complexes

Claudio Greco,[†] Giorgio Moro,[‡] Luca Bertini,[‡] Malgorzata Biczysko,[§] Vincenzo Barone,[§] and Ugo Cosentino*[,†]

[†]Dipartimento di Scienze dell'Ambiente e del Territorio e di Scienze della Terra, Università degli Studi di Milano-Bicocca; Piazza della Scienza 1, 20126 Milano, Italy

[‡]Dipartimento di Biotecnologie e Bioscienze, Università degli Studi di Milano-Bicocca; Piazza della Scienza 2, 20126 Milano, Italy

[§]Scuola Normale Superiore, Piazza dei Cavalieri 7, 56126 Pisa, Italy

Supporting Information

ABSTRACT: The adiabatic transition energies from the lowest triplet states of four Europium tris β-diketonate/phenantroline complexes have been determined in vacuo and in dicholomethane solution by the ΔSCF approach at the density functional theory level, using the PBE1PBE and the CAM-B3LYP hybrid functionals. The calculated adiabatic transition energies have been compared with the experimental 0−0 transitions of each complex determined from phosphorescence spectra of the corresponding Gd^{3+} complexes and followed by direct comparison between simulated and experimental spectra line shapes.

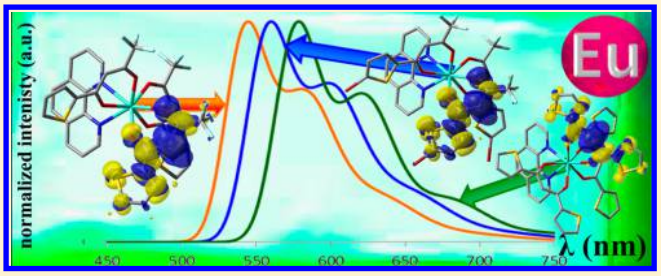

For compound **1**, the $Eu(TTA)_3Phen$ system, triplet states other than the lowest one and conformational isomers other than the one present in the crystallographic structure have been considered. In the crystallographic structure, this compound presents three quasi-degenerate low energy triplet states, differing for the TTA ligand where the two unpaired electrons are localized and showing close adiabatic transition energies. For compound **1**, the lowest triplet states of the four investigated conformational isomers show similar characteristics and close adiabatic transition energies. On the basis of these results, an investigation of compounds **2**−**4** ($Eu(Br\text{-}TTA)_3Phen$, $Eu(DTDK)_3Phen$, and $Eu(MeT\text{-}TTA)_3$) has been performed by considering only the isomer present in the crystallographic structure and only the lowest triplet state of each compound. For compounds **1**−**3**, the energies of the lowest triplet states calculated by both functionals in solution including zero-point energy corrections well reproduce the experimental trends as well as the values of the adiabatic transition energies: CAM-B3LYP, the best performing functional, provides energies of the lowest triplet state with deviations from experiments lower than 1200 cm^{-1}. Also, the calculated vibrationally resolved phosphorescence spectra and UV−vis absorptions well reproduce the main features of their experimental counterparts. Significant differences between calculated and experimental results are observed for compound **4**, for which difficulties in the experimental determination of the triplet state energy were encountered: our results show that the negligible photoluminescence quantum yield of this compound is due to the fact that the energy of the most stable triplet state is significantly lower than that of the resonance level of the Europium ion, and thus the energy transfer process is prevented. These results confirm the reliability of the adopted computational approach in calculating the energy of the lowest triplet state energy of these systems, a key parameter in the design of new ligands for lanthanide complexes presenting large photoluminescence quantum yields.

INTRODUCTION

Due to their photophysical properties, Lanthanide (Ln) complexes with π-conjugated ligands can act as light antennae, and thus find applications in several technological fields such as optoelectronic devices, sensors, bioassays and telecommunication.[1−4] In particular, europium complexes with β-diketonate (β-DK) ligands are attractive for optoelectronic applications because of their strong and narrow red emission.[5] The long luminescent lifetimes of Eu(III) ions are due to the forbidden character of their intra-4f transitions, which result in low absorption coefficients. The strategy generally adopted to overcome this problem foresees the sensitization procedure, involving the inclusion of the ion in a complex with a chromophore ligand. Upon excitation in an absorption band of the organic ligand, the excitation energy is transferred from the ligand to the lanthanide ion by intramolecular energy transfer. The commonly accepted energy migration path involved in sensitization forecasts that upon irradiation, the organic ligand is excited to the first excited singlet state S_1. By a nonradiative

Received: October 2, 2013
Published: December 23, 2013

Scheme 1

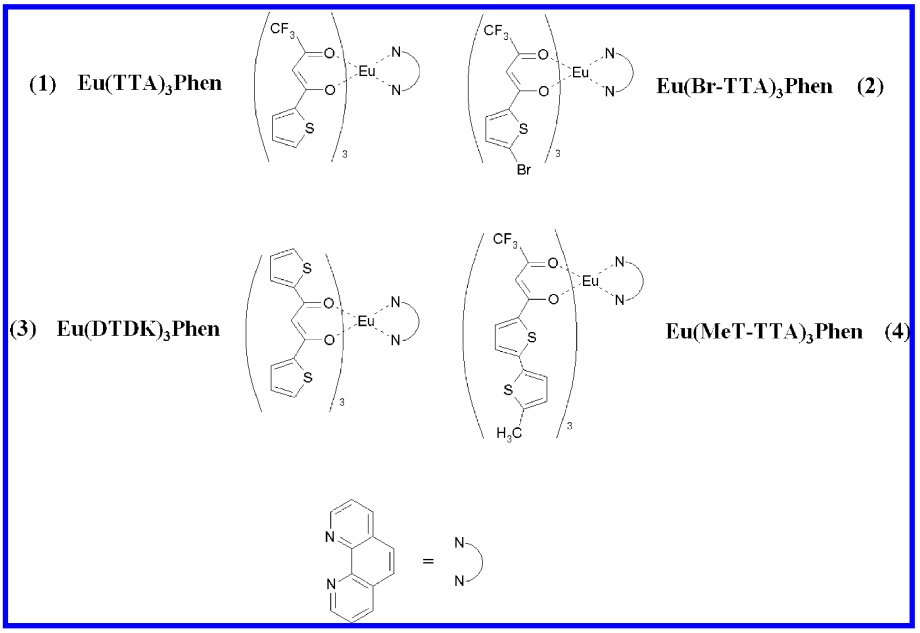

intersystem crossing, the S_1 excited state can decay to the T_1 triplet state and this may undergo a nonradiative transition to an excited state of the lanthanide ion (Ln*): the following radiative transition to a lower 4f state provides the characteristic line-like photoluminescence.

Lanthanide ion luminescence is only possible from the resonance levels of the ion: in the case of the Eu^{3+} ion, the resonance level corresponds to the $^5D_0$ level (17 300 cm^{-1}). To populate a resonance level, the lowest triplet state of the complex is required to be at an energy nearly equal or above the resonance level of the lanthanide ion. Because the position of the triplet level depends on the type of ligand, it is therefore possible to tune the luminescence intensity by variation of the ligand.

Photophysical requirements for highly emissive compounds are related to the energy transfer efficiency from the ligand to the ion and the minimization of collateral nonradiative processes. Some phenomenological rules have been proposed, relying on the simplified assumption that the $S_1-T_1-Ln^*$ energy transfer path is the only operative one and on considering that the only relevant parameter is the energy difference between the T_1 triplet state and the emitting resonance level of the lanthanide ion. On the basis of these assumptions, in the case of Eu(III) β-DK complexes, large photoluminescence quantum yields (PL-QY) are expected when the energy of the triplet state of the ligand is slightly above (2500−3500 cm^{-1}) the $^5D_1$ level of Eu(III), lying at 19 070 cm^{-1}.[3]

Quantum mechanical computations are providing remarkable contributions to rationalize the different photophysical pathways involved in sensitization process, as well as to provide a general way to screen antenna ligands.[6] In recent years, time-dependent density functional theory (TDDFT) has emerged as an accurate method, applicable to relatively large systems, for the calculation of excited state properties of molecules.[7−9] Thus, TDDFT appears to be an excellent approach for investigating the excited states of lanthanide(III) complexes. Moreover, inclusion of solvent effects in the TDDFT approach for calculation of both absorption and emission spectra[10,11] is now available and it represents a further improvement to achieve more reliable results. However, TDDFT limitations are to be considered. In particular, TDDFT provides unsatisfactory results when estimating excitation energies for Rydberg states and charge transfer transitions.[12,13] Continuous efforts are put in the development of new functionals, such as the hybrid exchange-correlation functional CAM-B3LYP (Coulomb attenuating method B3LYP)[13] that provides significant improvements in the description of these transitions.[14,15] Another limitation of TDDFT concerns the fact that double- or higher-excitations cannot be modeled by adiabatic TDDFT, because explicit many electron excitations are needed for a proper description of excitations of molecules with open-shell ground states.[16] For this reason, most of the TDDFT studies applied to Ln(III) complexes have been focused on the investigation of ligand-centered excited states, by using "large-core" relativistic effective core potentials (RECP), that is including 4f electrons in the core, to describe the Ln(III) ions.

Despite these limitations, DFT and TDDFT have been successfully applied to investigate absorption spectra of lanthanide(III) complexes as well as the relation between the triplet state energy and the luminescence properties of these systems.[17−21] The energy of the triplet state is generally obtained by the ΔSCF approach: as it is possible to perform geometry optimizations of a given system in its lowest triplet state, the excitation energy is estimated as the difference of the ground state S_0 energy, calculated at the ground state geometry, and the T_1 energy, calculated at the relaxed T_1 state geometry.

Also, semiempirical methods have been used for the characterization of the spectroscopic properties of lanthanide systems. Lanthanide ions are generally handled by using the Sparkle model, originally introduced for lanthanides in the AM1 method[22,23] and recently extended to the full lanthanide(III) series within the PM7 method,[24] or by the pseudocoordination center method, where the lanthanide ion is replaced with other "equivalent" ions (i.e., the pseudocenter) already present in the parametrization. Excited state calculations on lanthanide(III) complexes by using semiempirical methods have been mostly performed by using the INDO/S-CI approach,[25−29] and

dx.doi.org/10.1021/ct400865b | J. Chem. Theory Comput. 2014, 10, 767−777

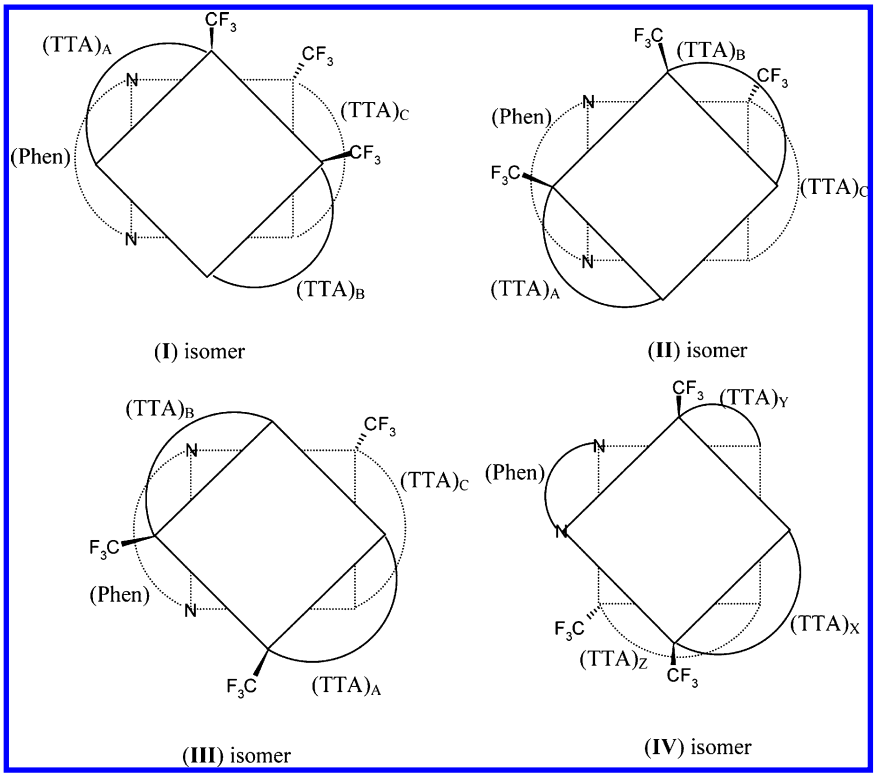

Figure 1. Sketch of the considered isomers of compound **1**, with adopted ligand labels. Top view of the square antiprismatic coordination: ligands sketched by curve lines; terminal CF_3 substituents highlighted.

provided reliable results on the characterization of the nature of the ligand triplet states, on the ordering of excited states and on the geometry variation of the ligand where the excitation is localized.

Despite the significant results obtained, semiempirical methods suffer from the general problem of dependence on the parametrization procedure (adopted molecular data set and included properties) and, in the specific case of lanthanides, from the lack of metal ion-ligand atom core interactions, which are only partially taken into account by the pseudocenter approach. Thus, it looks more significant to evaluate the ability of general ab initio approaches to investigate the spectroscopic properties of lanthanide systems.

Recently, a series of Europium tris β-DK/phenantroline complexes based on thienoyl ligands has been experimentally characterized in terms of photophysical properties, both in solid state (thin film) and CH_2Cl_2 solutions.[30] These systems, which present quite different photoluminescence quantum yields, represent an interesting benchmark for setting up computational strategies suitable to characterize the spectroscopic properties of lanthanide complexes.

Here we present the results of our theoretical investigation on the spectroscopic properties of the $Eu(TTA)_3Phen$ (**1**), $Eu(Br{-}TTA)_3Phen$ (**2**), $Eu(DTDK)_3Phen$ (**3**), and $Eu(MeT{-}TTA)_3Phen$ (**4**) complexes (see Scheme 1 for the ligand structures). Our attention was focused on the ability of computational methods to provide reliable values of the energy of the lowest triplet state of these compounds.

With this aim, calculations have been performed at the DFT level both in vacuo and including solvent effects by means of the Polarizable Continuum Model (PCM).[31] The energy of the lowest triplet state has been determined by the ΔSCF method and compared to the measured 0−0 transition of each complex, determined from the phosphorescence spectra of the frozen solution of the corresponding Gd^{3+} complexes. In the case of compound **1**, triplet states other than the lowest one and conformational isomers other than the one present in the crystallographic structure have been also investigated to test their influence on the spectroscopic properties of this system.

METHODS

All calculations on the investigated lanthanide complexes were performed with the Gaussian 09 program[32] in vacuo and in CH_2Cl_2 solution at the DFT level, using the hybrid functionals PBE1PBE[33] and CAM-B3LYP.[13] For lanthanide ions, large-core quasi-relativistic effective core potential (ECP) by Dolg et al.[34] and the related [5s4p3d]-GTO valence basis sets were used. For the ligand atoms, the 6-31G* basis set was used. Solvent effects were evaluated by the Gaussian 09 implementation of the PCM, using the C-PCM variant[35,36] and the UAHF solute cavity.[37]

The S_0 ground state and the T_1 lowest triplet state of all systems were optimized without symmetry constraints at the DFT level and frequency analysis was performed on the optimized geometries. Spin-unrestricted calculations were performed on the triplet states. DFT densities and energies are known to be less affected by spin contamination than the corresponding unrestricted Hartree−Fock quantities[38] and, in all the investigated systems, spin contamination was found to be negligible.

Energy gaps between T_1 (at the T_1 optimized geometry) and S_0 (at the S_0 optimized geometry), that is the $T_1 \rightarrow S_0$ adiabatic transition, were calculated including the zero point energy (ZPE) corrections. To get an overview of the nature of the T_1 state, TDDFT vertical transitions $T_1 \rightarrow S'_0$ were calculated at the T_1 optimized geometry. Electronic density map differences

dx.doi.org/10.1021/ct400865b | J. Chem. Theory Comput. 2014, 10, 767−777

Table 1. PBE1PBE Results for the T_1–T_4 States of Compound 1[a]

		ΔSCF			TDDFT			
state	unpaired electrons localization	adiabatic + ZPE (cm^{-1})	adiabatic no ZPE (cm^{-1})	vertical (cm^{-1})	vertical (cm^{-1})	starting MO	final MO	coeff
T_1	$(TTA)_B$	17721	18796	17782	16420	HOMO π $(TTA)_B$	LUMO π^* $(TTA)_B$	0.669
T_2	$(TTA)_C$	17845	18965	17820	16416	HOMO π $(TTA)_C$	LUMO π^* $(TTA)_C$	0.686
T_3	$(TTA)_A$	17964	19046	18038	16636	HOMO π $(TTA)_A$	LUMO π^* $(TTA)_A$	0.660
T_4	(Phen)	21440	22695	18903	15588	HOMO-3 π $(TTA)_{AC}$(Phen)	LUMO π^* (Phen)	0.462
						HOMO-2 π $(TTA)_{AB}$(Phen)	LUMO π^* (Phen)	0.339
						HOMO-1 π $(TTA)_{ABC}$	LUMO π^* (Phen)	0.187
						HOMO π $(TTA)_{BC}$(Phen)	LUMO π^* (Phen)	−0.313

[a]Ligand where unpaired electrons are localized (Mulliken analysis), and ΔSCF adiabatic ($T \rightarrow S_0$, with and without ZPE contribution) and vertical ($T \rightarrow S'_0$) transition energies calculated for the triplet state optimized structures. TDDFT results: vertical transition energies, MOs involved in vertical transitions, main relative coefficients in the CI expansion.

Table 2. PBE1PBE Results for the T_1–T_4 States of Compound 1[a]

	S_0	T_1 ΔR within $(TTA)_B$	S_0	T_2 ΔR within $(TTA)_C$	S_0	T_3 ΔR within $(TTA)_A$	S_0	T_4 ΔR within (Phen)
Eu–O_1	2.397	0.059	2.392	0.070	2.390	0.055		
O_1–C_1	1.266	0.007	1.268	0.004	1.268	0.006		
C_1–C_2	1.385	0.036	1.383	0.038	1.382	0.041		
C_2–C_3	1.418	0.024	1.420	0.023	1.421	0.019		
O_2–C_3	1.269	0.032	1.267	0.034	1.266	0.034		
Eu–O_2	2.404	−0.066	2.432	−0.076	2.437	−0.079		
C_3–C_4	1.464	−0.048	1.464	−0.048	1.464	−0.046		
C_1–(CF_3)	1.531	−0.018	1.530	−0.017	1.530	−0.018		
Eu–N_1							2.650	0.025
N_1–C_5							1.354	−0.032
C_5–C_6							1.444	0.042
C_6–N_2							1.354	−0.033
N_2–Eu							2.667	−0.057

[a]S_0 bond lengths (Å) and variations in the triplet state ($\Delta R = R_T - R_{S_0}$, Å) within the ligand where the two unpaired electrons are localized (refer to Scheme 2 for numbering of atoms in ligands).

(0.001 au) between the S'_0 (at the T_1 optimized geometry) and the T_1 states were also calculated. TDDFT calculations have been also performed on the S_0 ground state geometries to characterize UV–vis absorption spectra.

The vibrationally resolved phosphorescence spectra were calculated in the framework of the Franck–Condon (FC) approximation using the adiabatic Hessian (AH) model, in which both electronic states involved in the transition are treated on the same ground and the harmonic potential energy surfaces (PES) were calculated about their respective equilibrium geometries (see ref 39 and references therein for more details). Stick spectra were first generated and then convoluted using Gaussian distribution functions with half-widths at half-maxima of 500 cm^{-1}. Using the default parameters of the Gaussian 09 implementation, we obtained for the calculated intensity a fair convergence of the total computed intensity to the analytic value issuing from sum rules.[40,41] Although, by using more stringent thresholds, it is possible to obtain an improved convergence, this occurs at the expense of significantly increased computational times without any perceptible modification in the general appearance of the spectra.

RESULTS

Results on Eu(TTA)$_3$Phen. The crystallographic structure of $Eu(TTA)_3Phen$ presents a square antiprismatic coordination geometry around Eu(III) where six oxygen atoms from the three TTA ligands and two nitrogen atoms from the Phen ligand coordinate the central ion.[42] Figure 1 reports a molecular sketch of the different conformational isomers of this system considered in the present study, with the adopted ligand labels. The crystallographic structure of $Eu(TTA)_3Phen$ corresponds to the (**I**) isomer sketched in Figure 1.

Comparison of the S_0 optimized geometry with the crystallographic structure shows that PBE1PBE results in dichloromethane solution well reproduce the square antiprismatic coordination geometry around Eu(III) and the coordination bond distances (Supporting Information, Table 1S), confirming the reliability of the adopted theory level in predicting the structural feature of these systems, as it was previously observed also in the case of analogous Ytterbium(III) complexes.[43]

Preliminary TDDFT calculations on the optimized S_0 structure of compound **1** (Supporting Information, Table 2S) showed that the three lowest triplet states of this system (T_1–T_3) were very close in energy, falling within 250 cm^{-1}, the fourth triplet state being 2500 cm^{-1} less stable and the other ones at least 4800 cm^{-1} less stable.

The four lowest triplet states were considered in the following analysis. Each state was optimized at the TDDFT level and refined in the final steps of optimization by the ΔSCF method, after the considered triplet state had become the most stable one.

dx.doi.org/10.1021/ct400865b | J. Chem. Theory Comput. 2014, 10, 767–777

Mulliken atomic spin densities show that (Table 1) the two unpaired electrons are localized in each triplet state only on one ligand, that is on $(TTA)_B$, $(TTA)_C$, $(TTA)_A$, and (Phen), respectively (Figure 1). The four triplet states always present square antiprismatic coordination geometry, like in the ground state. With respect to S_0, a significant geometrical rearrangement is observed only within the ligand where the two unpaired electrons are localized (Tables 2 and 3S (Supporting Information)). In the T_1–T_3 states, a lengthening of the coordination Eu–O_1 bond distance (+0.06 Å) is observed together with a shortening (−0.08 Å) of the Eu–O_2 distance. The other bond distances within the coordination hexa-atomic ring increase whereas the formally single C_3–C_4 bond connecting the β-DK fragment to the thiophene moiety significantly decreases (−0.05 Å) and this is also the case, although to a lower extent, for the C_1–(CF_3) bond. No significant variations are observed within the phenanthroline fragment or in the Eu–N coordination bond distances. In the T_4 state, instead the β-DK fragments do not present significant bond distance variations with respect to S_0, whereas significant changes are observed for the Eu–N bonds and within the phenanthroline fragment.

Scheme 2

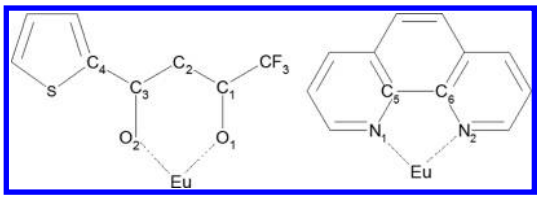

TDDFT calculations on the minimum energy geometries of the T_1–T_3 states show that the T → S'_0 vertical transitions mainly involve the π-HOMO and the π^*-LUMO of the TTA ligand where the two unpaired electrons are localized (Table 1). The same picture arises when the differences in the electron densities between the S'_0 (at the T optimized geometry) and the T states are considered (Figure 2): the electronic transition involves electron density rearrangement localized only on one ligand. In the case of T_4, the transition involves a charge transfer from MOs localized on the three TTA ligands to the LUMO on the phenanthroline fragment.

Finally, the adiabatic transition energies of the T_1–T_3 states are very close each other and fall within 250 cm^{-1} (Table 1), whereas the transition involving T_4 is 3700 cm^{-1} higher in energy. Comparison between T → S'_0 vertical and T → S_0 adiabatic (without ZPE contribution) transition energies, both calculated at the ΔSCF level, shows (Table1) the expected trend that is vertical energies lower than adiabatic ones. The observed differences in energies are about 3 kcal mol^{-1} in the T_1–T_3 cases and about 11 kcal mol^{-1} in the T_4 state. Comparison between vertical transition energies calculated at the ΔSCF-DFT and TDDFT levels shows the latter systematically lower than the ΔSCF ones: T_1–T_3 are lower by about 4 kcal mol^{-1}; T_4 by about 9 kcal mol^{-1}, making T_4 the most stable triplet state at the TDDFT level. As reported in Table 1, the MOs involved in the T_{1-3} → S'_0 transitions highlight an intraligand character, localized on a certain TTA ligand. Those involved in the T_4 case show instead an interligand character, with contributions from different MOs delocalized on all the four ligands. The delocalized character of this transition makes the TDDFT vertical energy much more sensitive to the well-known problems of this method when charge transfer transitions occur, and the fact that in ΔSCF-DFT this problem is partially overcome by the actual optimization of the LUMO makes T → S'_0 vertical ΔSCF-DFT values more reliable.

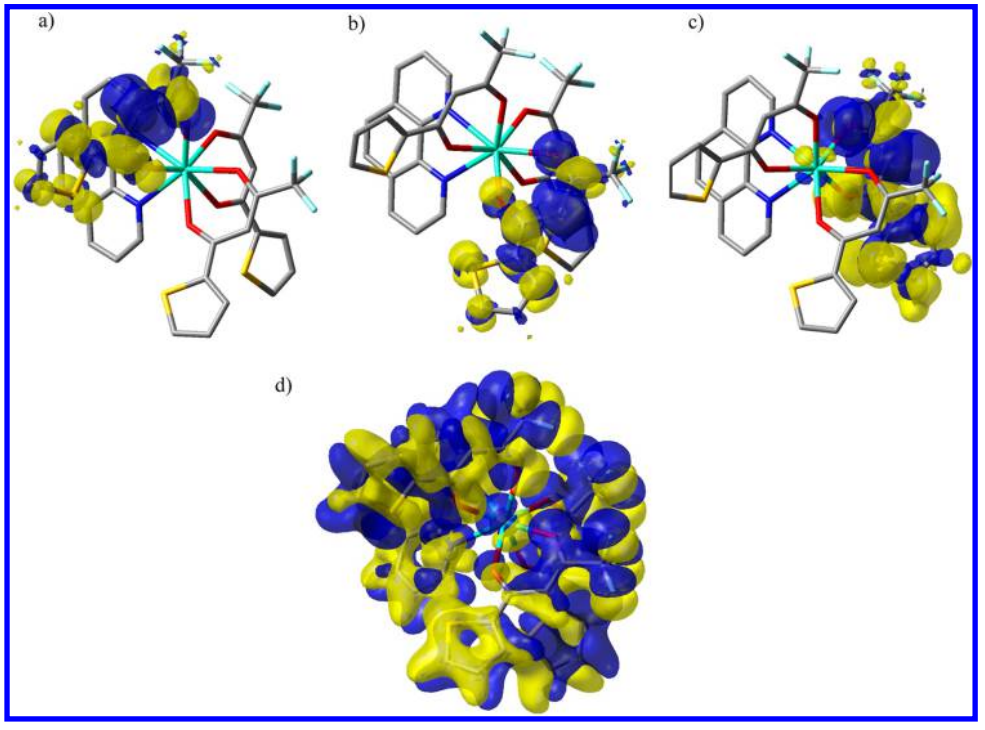

Figure 2. Electronic density map differences (0.001 au) for the optimized structures of T_1 (a), T_2 (b), T_3 (c), and T_4 (d) states of compound **1** (PBE1PBE results in solution) calculated between T and S'_0, at the T optimized geometry (yellow: positive values).

dx.doi.org/10.1021/ct400865b | J. Chem. Theory Comput. 2014, 10, 767–777

Table 3. PBE1PBE Results for the I–IV Isomers of Compound 1[a]

isomer	ΔE (kcal mol^{-1})	unpaired electrons localization	$T_1 \rightarrow S_0$ (cm^{-1})	TDDFT		
				starting MO	final MO	coeff
I	1.09	$(TTA)_B$	17721	HOMO π $(TTA)_B$	LUMO π^* $(TTA)_B$	0.669
II	0.32	$(TTA)_A$	17820	HOMO π $(TTA)_A$	LUMO π^* $(TTA)_A$	0.668
III	0.00	$(TTA)_B$	17869	HOMO π $(TTA)_B$	LUMO π^* $(TTA)_B$	0.668
IV	0.84	$(TTA)_Z$	17848	HOMO π $(TTA)_Z$	LUMO π^* $(TTA)_Z$	0.692

[a]Conformational energies (ΔE, including ZPE corrections); ligand where unpaired electrons are localized (Mulliken analysis) and $T_1 \rightarrow S_0$ adiabatic transition energies. TDDFT results: MOs involved in vertical transitions, and main relative coefficients in the CI expansion.

Table 4. PBE1PBE Results for the I–IV Isomers of Compound 1[a]

isomer	**I**		**II**		**III**		**IV**	
	S_0	T_1 ΔR within $(TTA)_B$	S_0	T_1 ΔR within $(TTA)_A$	S_0	T_1 ΔR within $(TTA)_B$	S_0	T_1 ΔR within $(TTA)_z$
Eu–O_1	2.397	0.059	2.406	0.060	2.409	0.075	2.409	0.073
O_1–C_1	1.266	0.007	1.266	0.007	1.267	0.006	1.267	0.006
C_1–C_2	1.385	0.036	1.384	0.037	1.384	0.037	1.383	0.037
C_2–C_3	1.418	0.024	1.419	0.022	1.419	0.022	1.419	0.022
O_2–C_3	1.269	0.032	1.268	0.033	1.267	0.034	1.267	0.035
Eu–O_2	2.404	−0.066	2.412	−0.069	2.408	−0.067	2.423	−0.068
C_3–C_4	1.464	−0.048	1.464	−0.048	1.463	−0.047	1.464	−0.048
C_1–(CF_3)	1.531	−0.018	1.530	−0.018	1.530	−0.017	1.531	−0.018

[a]S_0 bond lengths (Å) and variations in the T_1 state ($\Delta R = R_{T_1} - R_{S_0}$, Å) within the TTA ligand where the two unpaired electrons are localized (refer to Scheme 2 for numbering of atoms in ligands).

All these results highlight that this compound presents three quasi-degenerate low energy triplet states that differ for the TTA ligand where the two unpaired electrons are localized and that show a similar intraligand excitation character and close adiabatic transition energies. On the other hand, the fourth triplet state involves interligand excitation at significantly higher energy. Thus, to determine the energy of the lowest triplet state of these systems, we confidently assume that it can be achieved by considering only one (the lowest) triplet state.

Results on Conformational Isomers of Eu(TTA)$_3$Phen. Comparison of the crystallographic structures of Eu(TTA)$_3$Phen (**1**) and Eu(MeT–TTA)$_3$Phen (**3**) shows that these systems present a similar coordination geometry but with different reciprocal arrangements of the ligands around the ion. They correspond, respectively, to the **I** and **II** isomers sketched in Figure 1. Moreover, NMR analysis on compound **1** suggested[30] that in solution this complex can undergo a conformational rearrangement with respect to the isomer present in the crystal structure. These evidences prompted us to analyze the influence on the spectroscopic properties of the presence of different isomers for Eu(TTA)$_3$Phen.

The square antiprismatic geometry at the Eu(III) center, together with the bridging capabilities of TTA and 1,10-phenanthroline, could give rise to 32 enantiomeric pairs of isomers. Although an exhaustive investigation of all the isomers was not attempted, the three most interesting isomers **II**–**IV** (Figure 1) have been investigated in addition to the **I** isomer present in the crystallographic structure.

In the **I**–**III** isomers, each bidentate ligand occupies two adjacent vertices of one base of the antiprism; these three isomers differ by rotation of the upper plane with respect to the lower by 90°. In the **IV** isomer, phenantroline and one TTA ligand occupy two vertices belonging to different planes of the antiprism and adopt a "bridge" disposition.

Geometry optimization of the ground state of the considered isomers provides four stable structures, all presenting a square antiprismatic coordination geometry around the Eu(III). Isomers **I** and **II** correspond to the geometries present in the crystallographic structures of the Eu(TTA)$_3$Phen and Eu(MeT–TTA)$_3$Phen, respectively. The four isomers present comparable stability (Table 3), **III** being slightly more stable than the others, and all are expected to be present in dichloromethane solution.

On the basis of the results obtained in the previous section, geometry optimizations of the **II**–**IV** isomers were performed only for the most stable triplet states (T_1). Mulliken atomic spin densities show the two unpaired electrons localized in the four isomers only on one ligand, respectively on the $(TTA)_B$, the $(TTA)_A$, the $(TTA)_B$, and the $(TTA)_Z$ ligands (Figure 1). As observed above for the different triplet states of compound **1**, bond distance variations issuing from $S_0 \rightarrow T_1$ excitation involve only the TTA ligand where the two unpaired electrons are localized (Tables 4 and 4S (Supporting Information)). In particular, Eu–O_1 bond lengths increase (+0.07 Å), while Eu–O_2 distances decrease (−0.07 Å); the other distances within the hexa-atomic ring increase and the C_3–C_4 as well as the C_1–(CF_3) bond distances are shortened.

Analysis of the vertical $T_1 \rightarrow S'_0$ transitions at the TDDFT level shows that they mainly involve the π-HOMO and the π^*-LUMO of the TTA ligand where the two unpaired electrons are localized (Table 3). The same picture arises when the differences in the electron densities involved in the transitions are considered (Supporting Information, Figure 1S). Finally, the adiabatic transition energies calculated in solution for these isomers (Table 3) are very close and differ by no more than 150 cm^{-1}.

These results suggest that in solution this system presents a complex mixture of different isomers; nevertheless, the triplet states of these isomers show very similar characteristics and, more interestingly from our point of view, close adiabatic transition energies. Thus, for the other compounds only one

dx.doi.org/10.1021/ct400865b | J. Chem. Theory Comput. 2014, 10, 767–777

isomer, the one present in the crystallographic structure, has been considered in the following investigation.

Influence of Lanthanide Ion on Calculated Adiabatic Transition Energies. Experimental estimates of the energy of the lowest triplet state of lanthanide complexes are generally derived from measurements of the 0−0 transitions determined from the phosphorescence spectra of the frozen solution of the corresponding Gd^{3+} complexes.

To test the influence of the lanthanide ion on the adiabatic transition energies, calculations were performed on the $Gd(TTA)_3Phen$ system. Because the adiabatic transition energies calculated in solution for the Eu (17 721 cm^{-1}) and Gd (17 706 cm^{-1}) complexes are very similar, we can confidently compare the T_1 energies computed for the Eu systems with those obtained on the corresponding Gd complexes.

Results on Compounds 1−4. On the basis of the results discussed above, an investigation of compounds **2**−**4** has been performed by considering only the isomer present in the crystallographic structure and only the lowest triplet state of each compound. For compound **1**, results of the **I** isomer are considered in the following.

In the crystallographic structures, compounds **1** and **2** present the same ligand disposition around the Europium ion, corresponding to the **I** isomer of Figure 1, while compounds **3** and **4** prefer the **II** isomer. The S_0 ground state and the T_1 lowest triplet state of each system have been submitted to geometry optimization.

The equilibrium geometries of ground electronic states are always characterized by a square antiprismatic coordination around the Eu^{3+} ion. The calculated bond distances and coordination geometries compare well with those present in the crystallographic structures (Supporting Information, Table 1S): on average, the calculated Eu−N and the Eu−O bond distances are slightly underestimated (by 0.07 and 0.05 Å, respectively), with respect to the crystallographic values.

The experimental absorption spectra of compounds **1**−**4** in CH_2Cl_2 show[30] a broad band in the 310−450 nm range with a maximum (Table 5) in the 340−390 nm range and a shoulder at higher wavelengths in the 360−430 nm range, which have been attributed to different electronic transitions.[21] TDDFT calculations of vertical excitation energies on the S_0 ground state geometries provide the wavelengths of transitions involving the first 20 singlet states and Table 5 reports results for the most intense ones. Theoretical results show a satisfactory agreement with experimental spectra (Table 5): the calculated values show two main absorptions, the maximum being at lower wavelength than the shoulder. Separation between these signals is slightly underestimated by TDDFT, by about 20 nm. In general, the calculated absorbance wavelength results blueshifted by about 20 nm with respect to the corresponding experimental values.

Table 5. Calculated (TDDFT PBE1PBE Results) and Experimental[30] Absorption Spectra for Compounds 1−4[a]

	PBE1PBE		experimental	
	maximum λ (nm)	shoulder λ (nm)	maximum λ (nm)	shoulder λ (nm)
1	320 (1)	331 (0.69)	340	360
2	333 (1)	343 (0.61)	350	370
3	360 (1)	372 (0.24)	370	410
		366 (0.52)		
		365 (0.37)		
4	399 (1)	419 (0.20)	390	430
	399 (0.47)			
	394 (0.36)			

[a]Wavelength (λ, nm) of the maximum of absorbance and of the shoulder. Relative intensities in parentheses.

According to Zhang,[21] who investigated, among others also, the $Eu(TTA)_3Phen$ system at the DFT level, the $S_0 \rightarrow S_1$ transition (Supporting Information, Table 5S) mostly originates from the HOMO−LUMO transition, characterized by negligible oscillator strength (between 0.002 and 0.08). These transitions always involve, as starting and final MOs, MOs delocalized only on the beta-diketonate ligands.

The shoulders generally involve transitions from the S_0 to the S_2 state (Supporting Information, Table 6S). In the case of compounds **1** and **3**, these transitions involve starting MOs delocalized on the β-diketonate ligands, and final MOs delocalized also on the phenantroline ligand. In the case of compounds **2** and **4**, transitions do not involve MOs delocalized on the phenantroline ligand instead: the starting and the final MOs are only delocalized on the β-diketonate ligands. Transition corresponding to absorption maxima in the spectra involves states between S_4 and S_7; also in this case, transitions of compounds **1** and **3** involve MOs delocalized also on the phenantroline ligand, in contrast with the case of compounds **2** and **4**.

Mulliken atomic spin densities of the lowest triplet states (Table 6) show that the two unpaired electrons are localized on the $(TTA)_B$ and $(Br-TTA)_B$ ligand of the **I** isomer, and on the $(DTDK)_B$ and $(MeT)_B$ ligand of the **II** isomer. As previously observed, the coordination geometries of the lowest triplet states are similar to those of their corresponding ground states and the main differences are observed in the interatomic distances within the ligand where the two unpaired electrons are localized (Tables 7 and 1S (Supporting Information)). The trends in bond distances observed in $Eu(TTA)_3Phen$ (**1**) are found also in $Eu(Br-TTA)_3Phen$ (**2**): a consistent lengthening of the Eu−O_1 bonds (+0.06 Å) and shortening of the Eu−O_2 distances (−0.08 Å); a smaller increase of the other distances within the hexa-atomic rings and a decrease of the C_3-C_4 as well as the $C_1-(CF_3)$ bond distances. Compounds **3** and **4** present instead a slightly different picture: in compound **3** the Eu−O_1 and Eu−O_2 bond distances are very similar in S_0 and T_1 states; in compound **4**, the observed variations in the bond distances are smaller with respect to those of the other compounds, due to the larger delocalization ability of the DTDK ligand, as supported by the significantly lower spin density present on the β-DK fragment in compound **4** with respect to those found in the other compounds.

TDDFT results show (Table 6) that in all compounds the $T_1 \rightarrow S'_0$ vertical transitions mainly involve the π-HOMO and the π*-LUMO localized on the ligand where the two unpaired electrons are localized. Accordingly, differences in the electron densities between the S'_0 (at the T_1 optimized geometry) and the T_1 states (Figure 3) show that the electronic transition involves rearrangement localized only on one ligand.

With the aim of evaluating solvent effects on the adiabatic transitions energies, the S_0 and the T_1 states of compounds **1**−**4** have been optimized also in vacuo: the calculated $T_1 \rightarrow S_0$ adiabatic transitions energies are reported in Table 8, also highlighting the contribution of ZPE corrections. For comparison, the experimental 0−0 transition of each complex,

dx.doi.org/10.1021/ct400865b | J. Chem. Theory Comput. 2014, 10, 767−777

Table 6. PBE1PBE and CAM-B3LYP Results for Compounds 1−4[a]

		TDDFT		
	unpaired electrons localization	starting MO	final MO	coeff
PBE1PBE				
1	$(TTA)_B$	HOMO (π $TTA)_B$	LUMO (π^* $TTA)_B$	0.669
2	$(Br-TTA)_B$	HOMO (π $Br-TTA)_B$	LUMO (π^* $Br-TTA)_B$	0.679
3	$(DTDK)_B$	HOMO (π $DTDK)_B$	LUMO (π^* $DTDK)_B$	0.667
4	$(MeT)_B$	HOMO (π $MeT)_B$	LUMO (π^* $MeT)_B$	0.698
CAM-B3LYP				
1	$(TTA)_B$	HOMO (π $TTA)_B$	LUMO (π^* $TTA)_B$	0.662
2	$(Br-TTA)_B$	HOMO (π $Br-TTA)_B$	LUMO (π^* $Br-TTA)_B$	0.668
3	$(DTDK)_B$	HOMO (π $DTDK)_B$	LUMO (π^* $DTDK)_B$	0.654
4	$(MeT)_B$	HOMO (π $MeT)_B$	LUMO (π^* $MeT)_B$	0.746

[a]Ligand where unpaired electrons are localized (Mulliken analysis) and $T_1 \rightarrow S_0$ adiabatic transition energies. TDDFT results: MOs involved in vertical transitions, and main relative coefficients in the CI expansion.

Table 7. PBE1PBE Results for Compounds 1−4[a]

	$Eu(TTA)_3Phen$		$Eu(Br-TTA)_3Phen$		$Eu(DTDK)_3Phen$		$Eu(MeT)_3Phen$	
	S_0	T_1 ΔR within $(TTA)_B$	S_0	T_1 ΔR within $(Br-TTA)_B$	S_0	T_1 ΔR within $(DTDK)_B$	S_0	T_1 ΔR within $(MeT)_B$
$Eu-O_1$	2.397	0.059	2.399	0.063	2.399	−0.011	2.385	−0.002
O_1-C_1	1.266	0.007	1.265	0.002	1.277	0.014	1.269	0.006
C_1-C_2	1.385	0.036	1.386	0.027	1.404	0.039	1.382	0.001
C_2-C_3	1.418	0.024	1.416	0.025	1.405	0.036	1.422	0.002
O_2-C_3	1.269	0.032	1.269	0.034	1.275	0.014	1.269	0.016
$Eu-O_2$	2.404	−0.066	2.406	−0.078	2.392	−0.004	2.413	−0.036
$C_1-(CF_3)$	1.531	−0.018	1.530	−0.010			1.530	−0.005
C_3-C_4	1.464	−0.048	1.464	−0.060	1.472	−0.043	1.458	−0.026
$C'_3-C'_4$					1.471	−0.040		

[a]S_0 bond lengths (Å) and variations in the T_1 state ($\Delta R = R_{T_1} - R_{S_0}$, Å) within the ligand where the two unpaired electrons are localized (refer to Scheme 2 for numbering of atoms in ligands).

determined from the phosphorescence spectra of the frozen solution of the corresponding Gd^{3+} complex are reported since, as mentioned above, Gd and Eu complexes have very similar computed spectra.

PBE1PBE adiabatic transition energies calculated in vacuo without ZPE corrections nicely reproduce the experimental values, with the exception of compound **4**. However, inclusion of ZPE corrections and solvent effects cause a bathochromic shift of the calculated transition energies by about 1500 cm^{-1}. As a result, the most refined results obtained at the PBE1PBE level, i.e., including ZPE corrections and solvent effects, underestimate the experimental adiabatic transition energies by about 2300 cm^{-1}.

To test the role of the functional choice on the results, we repeated the computations by using the CAM-B3LYP model, which usually provides reliable spectroscopic parameters due to an improved description of long-range interactions. The adiabatic transition energies calculated for compounds **1**−**4** at the CAM-B3LYP level (Table 8) are larger than their PBE1PBE counterparts by about 1000 cm^{-1}. As for PBE1PBE results, ZPE corrections and solvent effects cause bathochromic shifts and, as a final result and with the exception of compound **4**, the CAM-B3LYP transition energies better reproduce the experimental values with a general underestimation lower than 1200 cm^{-1}.

As a further test of the reliability of the adopted computational procedure, the vibrationally resolved phosphorescence spectra of compounds **1**−**3** have been calculated in the framework of the Franck−Condon (FC) approximation at the CAM-B3LYP level. The experimental spectra present, besides the maximum of PL intensity, a shoulder at larger wavelengths (Table 9 and Figure S2 in ref 30), which, unlike the absorption spectra, do not result from other electronic transitions but are due to the vibronic structure of single electronic band. The calculated spectra (Figure 4 and Table 9) nicely reproduce the main features of the experimental spectra: the wavelength of maxima and shoulder results shifted by 40−50 nm toward higher wavelength with respect to the experimental ones but the relative sequence of peaks and their relative intensities agree well with the experimental data.

The calculated adiabatic transition energy of compound **4** significantly differs from the reported experimental value.[30] The experimental determination of the triplet state energy of this compound, which presents negligible PL-QY, was difficult[30] and a value of 19011 cm^{-1} was estimated. On the basis of this value, the authors suggested that the low PL-QY of the complex was justified by effective metal−ligand back energy transfer processes from the $^5D_1$ emitting level (19 070 cm^{-1}) to the triplet. Indeed, our results obtained with both functionals show that the energy of the triplet state (around 14 000 cm^{-1}) is significantly lower with respect to the estimated experimental value. Thus, the negligible PL-QY of this complex should be caused by the prevention of the energy transfer process due to the fact that the lowest triplet state is significantly lower than the resonance level of the Europium ion.

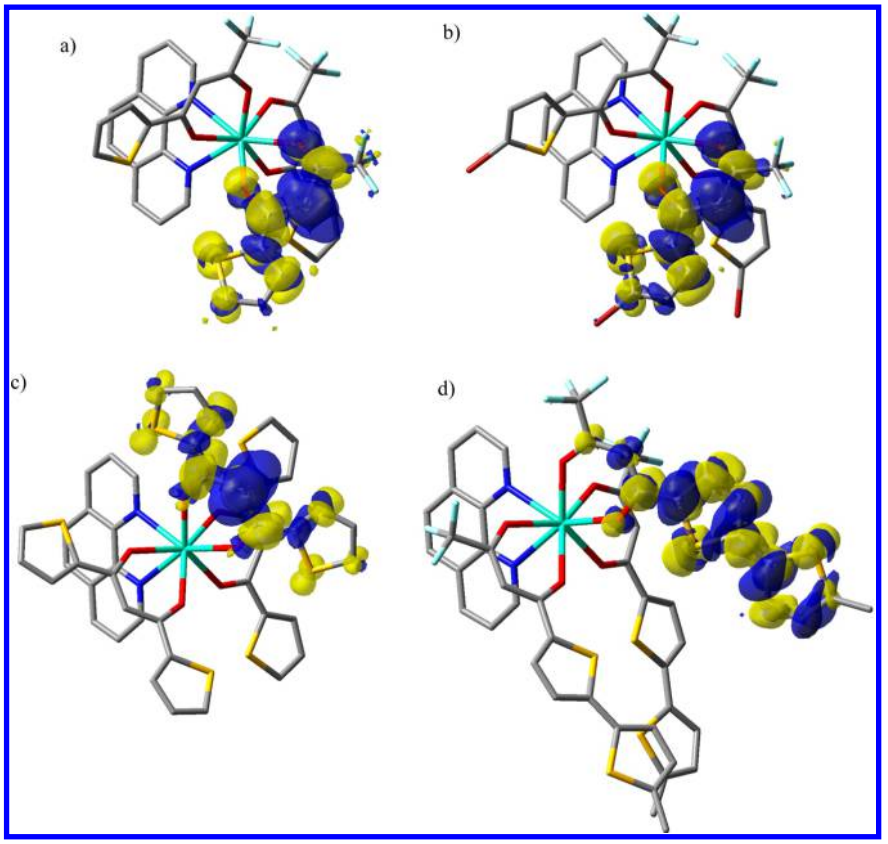

Figure 3. Electronic density map differences (0.001 au) for (a) $Eu(TTA)_3Phen$, (b) $Eu(Br\text{-}TTA)_3Phen$, (c) $Eu(DTDK)_3Phen$, and (d) $Eu(MeT{-}TTA)_3Phen$ complexes calculated at PBE1PBE level in solution between T_1 and S'_0, at the T_1 optimized geometry (yellow: positive values).

Table 8. PBE1PBE and CAM-B3LYP Results for Compounds 1−4[a]

	in vacuo		solution		experimental [Gd][30]
	no ZPE	+ZPE	no ZPE	+ZPE	
PBE1PBE					
$Eu(TTA)_3Phen$	19895	19051	18796	17721	19920
$Eu(Br\text{-}TTA)_3Phen$	19365	18539	18203	17017	19194
$Eu(DTDK)_3Phen$	18513	17746	17242	16233	18832
$Eu(MeT{-}TTA)_3Phen$	15280	14623	14601	14017	19011[b]
CAM-B3LYP					
$Eu(TTA)_3Phen$	20977	20122	19755	18665	19920
$Eu(Br{-}TTA)_3Phen$	20165	19393	19259	18156	19194
$Eu(DTDK)_3Phen$	20078	19231	18662	17480	18832
$Eu(MeT{-}TTA)_3Phen$	15677	14960	15273	14598	19011[b]

[a] $T_1 \rightarrow S_0$ ΔSCF adiabatic transition energies calculated on geometries optimized in vacuo and in solution with and without ZPE correction. Experimental 0−0 transitions from the corresponding Gd^{3+} complexes are also reported.[30] [b] Estimated experimental value.

Summarizing our results, we can state that the energies of the lowest triplet states calculated in solution including ZPE corrections for compounds **1**−**3** well reproduce the experimental trend, i.e., the differences between experimental energies are reproduced within 200 (CAM-B3LYP) and 400 (PBE1PBE) cm^{-1}. Moreover, the absolute values are calculated with satisfactory precision: the two functionals underestimate the experimental values by 1200 (CAM-B3LYP) and 2300 (PBE1PBE) cm^{-1}, respectively. Furthermore, the calculated vibrationally resolved phosphorescence spectra well reproduce the main feature of the experimental ones. Finally, the significant differences between calculated and experimental results on compound **4** should be ascribed to an overestimation of the experimental value caused by the difficulties encountered during the experimental determination.

CONCLUSIONS

One of the most critical parameters tuning the photoluminescence quantum yields in the photophysical pathways involved in sensitization process of luminescent lanthanide complexes is the energy difference between the T_1 triplet state of the complex and the emitting resonance level of the lanthanide. This prompted us to investigate a series of well-characterized europium β-diketonate complexes in order to set up and validate a reliable yet effective computational procedure

dx.doi.org/10.1021/ct400865b | J. Chem. Theory Comput. 2014, 10, 767−777

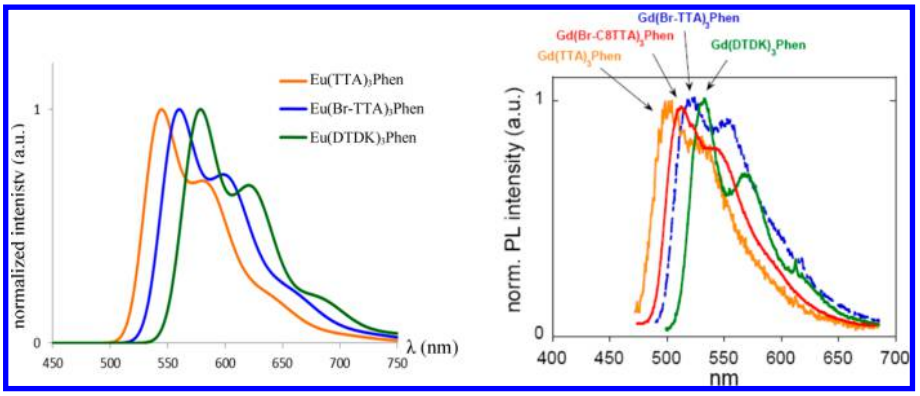

Figure 4. Calculated (CAM-B3LYP results) and experimental (from ref 30) phosphorescence spectra in solution for compounds **1**−**3** (normalized intensities).

Table 9. Calculated (CAM-B3LYP Results) and Experimental[30] Phosphorescence Spectra for Compounds 1−3[a]

	CAM-B3LYP		experimental	
	maximum	shoulder	maximum	shoulder
1	544 (1)	580 (0.69)	500 (1)	530 (0.81)
2	560 (1)	598 (0.72)	520 (1)	555 (0.93)
3	578 (1)	620 (0.67)	540 (1)	570 (0.68)

[a]Wavelength (nm) of the maximum of PL and of the shoulder. Relative intensities are in parentheses.

aimed to systematic studies of the spectroscopic characteristics of lanthanide complexes.

The results obtained for compound **1**, for which triplet states other than the lowest one and conformational isomers other than the one present in the crystallographic structure have been investigated, allow us to verify that investigation of the considered spectroscopic properties of these systems can be confidently restricted to the analysis of only the lowest triplet state of the isomer present in the crystallographic structure of each system.

Adopting this approach, the adiabatic transition energies calculated for compounds **1**−**3** well reproduce the experimental trend, with deviations from experiments lower than 1200 cm^{-1}; moreover, the calculated phosphorescence spectra nicely reproduce the experimental ones.

Both the adopted functionals deliver consistent results, with CAM-B3LYP providing the best performances in terms of triplet energies. Moreover, our results allow us to shed light also on the behavior of compound **4**, whose experimental determination faces against significant difficulties.

In conclusion, our results confirm the reliability of the adopted computational approach in calculating the energy of the lowest triplet state energy of these systems, a key parameter in the design of new ligands for lanthanide complexes presenting large photoluminescence quantum yields.

■ ASSOCIATED CONTENT

Supporting Information

Additional information on the electronic structure and geometric parameters of the models, as well as TDDFT computed excitation energies of compound **1** and TDDFT absorptions of compounds **1**−**4**. This material is available free of charge via the Internet at http://pubs.acs.org.

■ AUTHOR INFORMATION

Corresponding Author

*U. Cosentino. E-mail: ugo.cosentino@unimib.it. Tel.: 00390264482822.

Notes

The authors declare no competing financial interest.

■ ACKNOWLEDGMENTS

We gratefully acknowledge financial support from Milano-Bicocca University (FAR2012-2013).

■ REFERENCES

(1) Buenzli, J. C. G.; Piguet, C. *Chem. Soc. Rev.* **2005**, *34*, 1048−1077.
(2) Buenzli, J.-C. G. *Chem. Rev.* **2010**, *110*, 2729−2755.
(3) Eliseeva, S. V.; Buenzli, J.-C. G. *Chem. Soc. Rev.* **2010**, *39*, 189−227.
(4) Binnemans, K. *Chem. Rev.* **2009**, *109*, 4283−4374.
(5) Binnemans, Koen. In *Handbook on the Physics and Chemistry of Rare Earths*; Gschneidner, Karl A., Jr., Bünzli, Jean-Claude, Pecharsky, Vitalij K., Eds.; **2005**; Vol. *35*, pp 107−272.
(6) Platas-Iglesias, Carlos; Roca-Sabio, Adrián; Regueiro-Figueroa, Martín; Esteban-Gómez, David; de Blas, Andrés; Rodríguez-Blas, Teresa. *Curr. Inorg. Chem.* **2011**, *1*, 91−116.
(7) Stratmann, R. E.; Scuseria, G. E.; Frisch, M. J. *J. Chem. Phys.* **1998**, *109*, 8218−8224.
(8) Bauernschmitt, R.; Ahlrichs, R. *Chem. Phys. Lett.* **1996**, *256*, 454−464.
(9) Casida, M. E.; Jamorski, C.; Casida, K. C.; Salahub, D. R. *J. Chem. Phys.* **1998**, *108*, 4439−4449.
(10) Barone, V.; Improta, R.; Rega, N. *Acc. Chem. Res.* **2008**, *41*, 605−616.
(11) Scalmani, G.; Frisch, M. J.; Mennucci, B.; Tomasi, J.; Cammi, R.; Barone, V. *J. Chem. Phys.* **2006**, *124*, 94107.
(12) Dreuw, A.; Head-Gordon, M. *J. Am. Chem. Soc.* **2004**, *126*, 4007−4016.
(13) Yanai, T.; Tew, D. P.; Handy, N. C. *Chem. Phys. Lett.* **2004**, *393*, 51−57.
(14) Isegawa, M.; Peverati, R.; Truhlar, D. G. *J. Chem. Phys.* **2012**, *137*, 244104.
(15) Peach, M. J. G.; Helgaker, T.; Salek, P.; Keal, T. W.; Lutnaes, O. B.; Tozer, D. J.; Handy, N. C. *Phys. Chem. Chem. Phys.* **2006**, *8*, 558−562.
(16) Cox, H.; Stace, A. J. *Int. Rev. Phys. Chem.* **2010**, *29*, 555−588.
(17) Gutierrez, F.; Tedeschi, C.; Maron, L.; Daudey, J. P.; Poteau, R.; Azema, J.; Tisnes, P.; Picard, C. *Dalton Trans.* **2004**, 1334−1347.
(18) Guillaumont, D.; Bazin, H.; Benech, J.-M.; Boyer, M.; Mathis, G. *ChemPhysChem* **2007**, *8*, 480−488.
(19) Aiga, F.; Iwanaga, H.; Amano, A. *J. Phys. Chem. A* **2007**, *111*, 12141−12145.

(20) De Silva, C. R.; Li, J.; Zheng, Z.; Corrales, L. R. *J. Phys. Chem. A* **2008**, *112*, 4527−4530.
(21) Li, X.-N.; Wu, Z.-J.; Si, Z.-J.; Liang-Zhou; Liu, X.-J.; Zhang, H.-J. *Phys. Chem. Chem. Phys.* **2009**, *11*, 9687−9695.
(22) Deandrade, A.; Dacosta, N.; Simas, A.; Desa, G. *Chem. Phys. Lett.* **1994**, *227*, 349−353.
(23) Deandrade, A.; Dacosta, N.; Simas, A.; Desa, G. *J. Alloys Compd.* **1995**, *225*, 55−59.
(24) Dutra, J. D. L.; Filho, M. A. M.; Rocha, G. B.; Freire, R. O.; Simas, A. M.; Stewart, J. J. P. *J. Chem. Theory Comput.* **2013**, *9*, 3333−3341.
(25) Scotognella, F.; Meinardi, F.; Ottonelli, M.; Raimondo, L.; Tubino, R. *J. Lumin.* **2009**, *129*, 746−750.
(26) Destri, S.; Pasini, M.; Porzio, W.; Rizzo, F.; Dellepiane, G.; Ottonelli, M.; Musso, G.; Meinardi, F.; Veltri, L. *J. Lumin.* **2007**, *127*, 601−610.
(27) Ottonelli, M.; Izzo, G. M. M.; Rizzo, F.; Musso, G.; Dellepiane, G.; Tubino, R. *J. Phys. Chem. B* **2005**, *109*, 19249−19256.
(28) De Sa, G. F.; Malta, O. L.; Donega, C. D.; Simas, A. M.; Longo, R. L.; Santa-Cruz, P. A.; da Silva, E. F. *Coord. Chem. Rev.* **2000**, *196*, 165−195.
(29) Faustino, W. M.; Malta, O. L.; Teotonio, E. E. S.; Brito, H. F.; Simas, A. M.; de Sa, G. F. *J. Phys. Chem. A* **2006**, *110*, 2510−2516.
(30) Freund, C.; Porzio, W.; Giovanella, U.; Vignali, F.; Pasini, M.; Destri, S.; Mech, A.; Di Pietro, S.; Di Bari, L.; Mineo, P. *Inorg. Chem.* **2011**, *50*, 5417−5429.
(31) Tomasi, J.; Mennucci, B.; Cammi, R. *Chem. Rev.* **2005**, *105*, 2999−3094.
(32) Frisch, M. J.; Trucks, G. W.; Schlegel, H. B.; Scuseria, G. E.; Robb, M. A.; Cheeseman, J. R.; Scalmani, G.; Barone, V.; Mennucci, B.; Petersson, G. A.; Nakatsuji, H.; Caricato, M.; Li, X.; Hratchian, H. P.; Izmaylov, A. F.; Bloino, J.; Zheng, G.; Sonnenberg, J. L.; Hada, M.; Ehara, M.; Toyota, K.; Fukuda, R.; Hasegawa, J.; Ishida, M.; Nakajima, T.; Honda, Y.; Kitao, O.; Nakai, H.; Vreven, T.; Montgomery, J. A., Jr.; Peralta, J. E.; Ogliaro, F.; Bearpark, M.; Heyd, J. J.; Brothers, E.; Kudin, K. N.; Staroverov, V. N.; Keith, T.; Kobayashi, R.; Normand, J.; Raghavachari, K.; Rendell, A.; Burant, J. C.; Iyengar, S. S.; Tomasi, J.; Cossi, M.; Rega, N.; Millam, J. M.; Klene, M.; Knox, J. E.; Cross, J. B.; Bakken, V.; Adamo, C.; Jaramillo, J.; Gomperts, R.; Stratmann, R. E.; Yazyev, O.; Austin, A. J.; Cammi, R.; Pomelli, C.; Ochterski, J. W.; Martin, R. L.; Morokuma, K.; Zakrzewski, V. G.; Voth, G. A.; Salvador, P.; Dannenberg, J. J.; Dapprich, S.; Daniels, A. D.; Farkas, O.; Foresman, J. B.; Ortiz, J. V.; Cioslowski, J.; Fox., D. J. *Gaussian 09* revision C.01; Gaussian, Inc.: Wallingford, CT, 2010, 2011.
(33) Adamo, C.; Barone, V. *J. Chem. Phys.* **1999**, *110*, 6158−6170.
(34) Dolg, M.; Stoll, H.; Preuss, H. *Theor. Chim. Acta* **1989**, *75*, 173−194.
(35) Barone, V.; Cossi, M. *J. Phys. Chem. A* **1998**, *102*, 1995−2001.
(36) Cossi, M.; Rega, N.; Scalmani, G.; Barone, V. *J. Comput. Chem.* **2003**, *24*, 669−681.
(37) Barone, V.; Cossi, M.; Tomasi, J. *J. Chem. Phys.* **1997**, *107*, 3210−3221.
(38) Menon, A. S.; Radom, L. *J. Phys. Chem. A* **2008**, *112*, 13225−13230.
(39) Biczysko, M.; Bloino, J.; Santoro, F.; Barone, V. In *Computational Strategies for Spectroscopy*; Barone, V., Ed.; John Wiley & Sons, Inc.: New York, 2011; pp 361−443.
(40) Barone, V.; Bloino, J.; Biczysko, M.; Santoro, F. *J. Chem. Theory Comput.* **2009**, *5*, 540−554.
(41) Bloino, J.; Biczysko, M.; Santoro, F.; Barone, V. *J. Chem. Theory Comput.* **2010**, *6*, 1256−1274.
(42) Hu, M. L.; Huang, Z. Y.; Cheng, Y. Q.; Wang, S.; Lin, J. J.; Hu, Y.; Xu, D. J.; Xu, Y. Z. *Chin. J. Chem.* **1999**, *17*, 637−643.
(43) Sanguineti, A.; Monguzzi, A.; Vaccaro, G.; Meinardi, F.; Ronchi, E.; Moret, M.; Cosentino, U.; Moro, G.; Simonutti, R.; Mauri, M.; Tubino, R.; Beverina, L. *Phys. Chem. Chem. Phys.* **2012**, *14*, 6452−6455.